Research Paper

Design of Internalizing PSMA-specific Glu-ureido-based Radiotherapeuticals

Till Wüstemann[1], Ulrike Bauder-Wüst[2], Martin Schäfer[2], Matthias Eder[2], Martina Benesova[2], Karin Leotta[1], Clemens Kratochwil[1], Uwe Haberkorn[1,3], Klaus Kopka[2,3] and Walter Mier[1✉]

1. AffiliationDepartment for Nuclear Medicine, Heidelberg University Hospital, Im Neuenheimer Feld 400, 69120 Heidelberg, Germany
2. Division of Radiopharmaceutical Chemistry, German Cancer Research Center (DKFZ), Heidelberg, Germany
3. German Cancer Consortium (DKTK), Heidelberg, Germany.

✉ Corresponding author: email: walter.mier@med.uni-heidelberg.de

Abstract

Despite the progress in diagnosis and treatment, prostate cancer (PCa) is one of the main causes for cancer-associated deaths among men. Recently, prostate-specific membrane antigen (PSMA) binding tracers have revolutionized the molecular imaging of this disease. The translation of these tracers into therapeutic applications is challenging because of high PSMA-associated kidney uptake. While both the tumor uptake and the uptake in the kidneys are PSMA-specific, the kidneys show a more rapid clearance than tumor lesions. Consequently, the potential of endoradiotherapeutic drugs targeting PSMA is highly dependent on a sustained retention in the tumor - ideally achieved by predominant internalization of the respective tracer. Previously, we were able to show that the pharmacokinetics of the tracers containing the Glu-urea-based binding motif can be further enhanced with a specifically designed linker. Here, we evaluate an eventual influence of the chelator moiety on the pharmacokinetics, including the tumor internalization. A series of tracers modified by different chelators were synthesized using solid phase chemistry. The conjugates were radiolabeled to evaluate the influence on the receptor binding affinity, the ligand-induced internalization and the biodistribution behavior. Competitive binding and internalization assays were performed on PSMA positive LNCaP cells and the biodistribution of the most promising compound was evaluated by positron emission tomography (PET) in LNCaP-tumor-bearing mice. Interestingly, conjugation of the different chelators did not cause significant differences: all compounds showed nanomolar binding affinities with only minor differences. PET imaging of the ^{68}Ga-labeled CHX-A''-DTPA conjugate revealed that the chelator moiety does not impair the specificity of tumor uptake when compared to the gold standard PSMA-617. However, strong differences of the internalization ratios caused by the chelator moiety were observed: differences in internalization between 15% and 65% were observed, with the CHX-A''-DTPA conjugate displaying the highest internalization ratio. A first-in-man PET/CT study proved the high tumor uptake of this ^{68}Ga-labeled PSMA-targeting compound. These data indicate that hydrophobic entities at the chelator mediate the internalization efficacy. Based on its specific tumor uptake in combination with its very high internalization ratio, the clinical performance of the chelator-conjugated Glu-urea-based PSMA inhibitors will be further elucidated.

Key words: prostate-specific membrane antigen, PSMA, tumor targeting, prostate cancer, chelators, theranostics, positron emission tomography

Introduction

Prostate cancer (PCa) persists to be one of the main causes for cancer related deaths among men. Diagnostics of PCa is challenging because early tumor stages usually do not cause symptoms. Given the poor sensitivity and predictive value of CT/MRI for extraprostatic disease, PCa diagnosis mainly relies on the blood tumor marker prostate-specific antigen (PSA) [1].

[11]C-choline, ^{18}F-fluorocholine and ^{18}F-fluorome-thylcholine remain hitherto the most promising PET/CT imaging agents that were able to detect PCa sufficiently yet not optimally [2-4]. Once metastasized PCa is no longer curable by surgical and external radiation therapies and the treatment option of choice remains hormone therapy. However, after some years most patients do no longer respond to hormone therapy and metastatic castration-resistant prostate cancer presents with a poor survival rate [5] owing to rare therapeutic options [6] and observed ineffectiveness of chemotherapy with taxanes because of early resistance and severe side effects [7].

Improved therapeutic efficacy might be achieved with drugs specifically targeting prostate tumors. Due to its tumor specific expression the prostate-specific membrane antigen (PSMA) represents an ideal biological target. PSMA is a membrane bound peptidase belonging to the type II transmembrane protein family. It is expressed in almost all types of prostate tumors with increased amounts in metastatic, poorly differentiated and hormone-refractory tumors. [8] In these tissues, its expression level is up to 1000-fold higher as compared to physiological levels found in kidney, small intestine and in the brain [9, 10] where PSMA is also named folate hydrolase 1 [11], N-acetylated α-linked acidic dipeptidase (NAALADase) [12, 13] or glutamate carboxypeptidase II [14]. Moreover, the expression levels of PSMA correlate with the progression of the disease [15]. It internalizes upon binding to a specific ligand up to threefold in comparison to the basal internalization level [16].

For the noninvasive detection of occult PCa ProstaScint®, a PSMA binding antibody was developed [17]. This ^{111}In labeled tracer, however, suffered from the poor pharmacokinetics caused by its high molecular weight and from the fact that it recognizes only an intracellular epitope of the protein [18, 19]. In former studies it has been shown that Glu-urea-based inhibitors show high affinity to PSMA [20]. The first imaging agents derived from this structure were labeled with radioactive halogen isotopes and showed nanomolar binding affinity, resulting in excellent imaging properties [21, 22]. In subsequent studies ligands labeled with radiometals were designed such as [^{68}Ga]Ga-Glu-urea-Lys-(Ahx)-HBED-CC (in short: ^{68}Ga-PSMA-11). This PSMA ligand provides high detection rates even at low PSA levels [23-28].

These compounds showed enhanced imaging properties for the detection and clinical monitoring of prostate tumors [22, 25, 26, 29]. The excellent contrast between the tumor and normal tissues indicates a high potential of PSMA based therapy. Subsequently,

first studies using therapeutic radionuclides were conducted [30, 31]. The basis for an efficient therapy is a selective uptake combined with a high ratio of internalization to prolong the exposure of the tumor to the decaying radionuclide. While all therapeutics currently in development show high binding affinity to PSMA *in vitro*, they often lack high ratios of internalization. The most potent ligands currently known for therapy with radiometals comprise the Glu-urea-based binding motif and the chelator coupled via a linker. There is increasing evidence about the synergistic effect of the linker moiety on the overall binding of PSMA ligands. Consequently, a study tested different linkers and found that a linker moiety containing 2-naphthyl-L-alanine showed the best performance *in vitro* and *in vivo* [32].

Now, the aim of this work is to study the influence of the chelator moiety on PSMA ligands in detail. The compounds studied included the recently first-in-man examined DOTA-coupled compound PSMA-617 [30] and the compound coupled to HBED-CC (PSMA-11) - a highly efficient tracer for PET imaging of PCa [26, 29].

Experimental

Synthesis of the PSMA binding motif

All chemicals were of analytical grade and were used without further purification. If not otherwise denoted, chemicals were purchased from Sigma-Aldrich, Munich, Germany or Merck, Darmstadt, Germany. The general synthesis procedure has been described in detail [27, 33], the details can be found in the supplemental material. In short, Fmoc-Lys(Alloc)-OH (Orpegen Peptide Chemicals GmbH, Heidelberg, Germany) was immobilized on 2-chlorotritylresin. H-Glu-(O*t*Bu)-O*t*Bu × HCl was coupled with triphosgene yielding the isocyanate of the glutamyl moiety. After capping of the resin and cleavage of the Fmoc group of the lysine, the isocyanate was added. Next, the Alloc-group was cleaved using the Pd catalyst tetrakis(triphenylphosphine)palladium(0).

Coupling of the linker moiety

The linker moiety comprises a 2-naphthyl-L-alanine and *trans*-4-(aminomethyl) cyclohexanecarboxylic acid. Coupling was achieved using standard peptide synthesis.

General procedure for the coupling of the PSMA binding motif to different chelators

The chelators presented in figure 1 were coupled to the linker by solid phase synthesis. In detail, the PSMA binding motif coupled to the resin was deprotected using 20% piperidine in DMF.

Subsequently, 2 to 4 equivalents of the chelator (depending on the reactivity of the chelator), 0.98 × $n_{chelator}$ 1-[bis(dimethylamino)methylene]-1*H*-1,2,3-triazolo[4,5-*b*]pyridinium 3-oxid hexafluorophosphate (HATU) (if required) and 10 equivalents of DIPEA, dissolved in 500 µl of DMF were added and incubated for 16 h. The exact reaction conditions for every chelator are listed in table 1. In order to obtain the highly lipophilic derivative of the conjugate coupled to bis((1-(carboxymethyl)-1H-imidazol-2-yl)methyl)amino (CIM), the Fmoc group was not removed.

The progress of the reaction was monitored by HPLC analysis of test samples. Subsequently, the peptide was cleaved from the resin. The cleavage mixture contained 95% trifluoroacetic acid (TFA, Biosolve, Valkenswaard, the Netherlands), 2.5% H_2O and 2.5% triisopropylsilane (TIPS).

Purification was achieved by preparative HPLC (gradients are specified in table 1). The purified compounds were analyzed by analytical HPLC (0 – 100% MeCN in water within 5 min, Monolith RP HPLC column 100 × 3 mm (Merck, Darmstadt, Germany) and LC/MS (Thermo Scientific Exactive Plus Orbitrap, Thermo Fisher Scientific Inc., Waltham, USA). The product fractions were pooled and lyophilized.
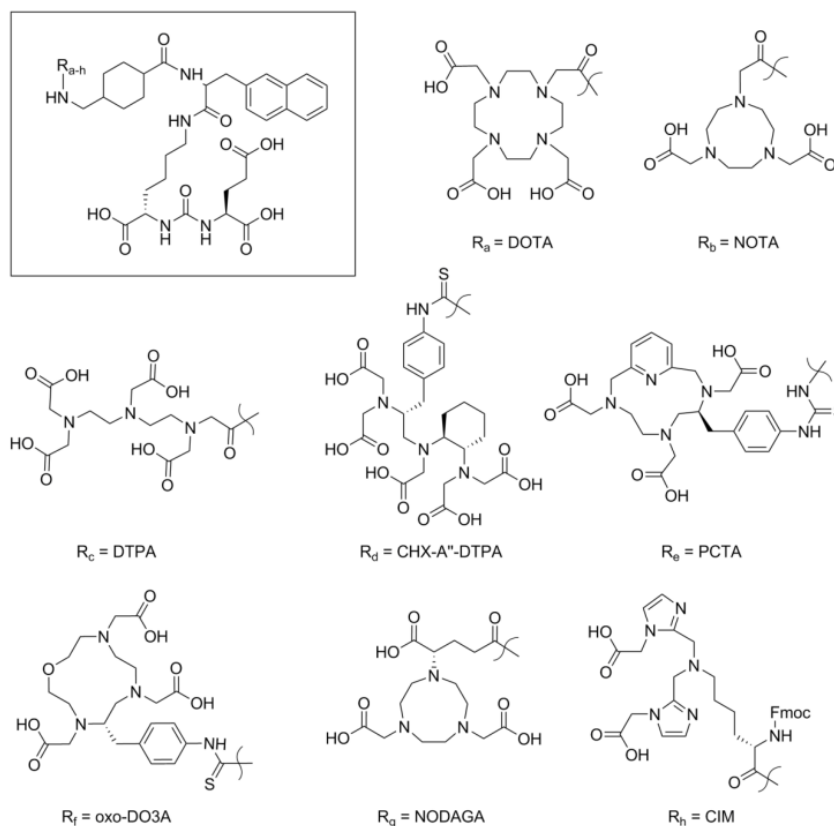

Figure 1: Chemical structures of the binding motif (framed) and the chelator moieties used to study the effect of the distant building block in the PSMA binding conjugates.

Table 1: Specifications of the reaction conditions applied in the conjugation high yields of the final compound. All reactions were carried out for 16 h. For the coupling of NODAGA triethylamine (TEA) was used instead of DIPEA.

	DOTA	NOTA	DTPA	CHX-A''-DPTA	PCTA	Oxo-DO3A	NODAGA	CIM
Chelator precursor	DOTA-*p*-nitro-phenol ester	NOTA-difluor-phenol ester	DTPA-tetra (*t*-butyl ester)	CHX-A''-DTPA isothio-cyanate	PCTA-isothio-cyanate	Oxo-DO3A isothio-cyanate	NODAGA isothio-cyanate	CIM
Equivalents Chelator	4	2	2	3	2	2	2	2
Equivalents DIPEA	20	10	10	10	16	16	10 (TEA)	10
Equivalents HATU	-	-	1.96	-	-	-	-	1.90
Purification gradient	10-40% ACN	10-40% ACN	10-40% ACN	20-50% ACN	15-45% ACN	15-45% ACN	15-45% ACN	25-55% ACN

[177]Lu-labeling of DOTA, NOTA, CHX-A''-DTPA, PCTA, oxo-DO3A and NODAGA-conjugates

[177]LuCl$_3$ (100 MBq, Perkin Elmer Inc., Waltham, USA) was mixed with 200 µl of 0.4 M sodium acetate buffer containing Chelex (pH = 5, Bio-Rad Laboratories GmbH, Munich, Germany). 10 µl of a 1 mM solution of the compound in 10% DMSO in water, 2 µl of a saturated solution of ascorbic acid and 40 µl of the solution containing ^{177}Lu were mixed and heated to 95 °C for 10 min. The labeling was checked by radio-HPLC (0 – 100% MeCN in water within 5 min, Monolith column).

[125]I-labeling of MIP-1095

30 MBq of [125]I (Perkin Elmer Inc., Waltham, USA) were mixed with 5 µl of a MIP-1095-Sn solution (Progenics Pharmaceuticals, New York, USA) containing 0.25 mg precursor/ml in ethanol and 2.5 µl of 4.5% H$_2$O$_2$ in glacial acetic acid. After 1 min incubation the reaction was checked by radio HPLC (0 – 100% MeCN in water within 5 min, on the Monolith RP HPLC) and afterwards taken up into a SOLA cartridge. The cartridge was washed with water and eluted with 500 µl TFA. The TFA solution was incubated for 7 minutes, mixed with water and loaded onto a Bond Elut cartridge. Washing was performed with 20% ethanol in water and the product was eluted with 1 ml ethanol. The ethanol was evaporated in vacuo and the product dissolved in 150 µl of 0.9% NaCl in water. The result of the labeling was checked by radio HPLC (0 – 100% MeCN in water within 5 min, Monolith column).

[99m]Tc-labeling of CIM-conjugate

CIM-conjugate was labeled using a [99m]Tc(CO)$_3$ core using a CRS tricarbonyl labeling kit (PSI, Zürich, Switzerland). 400 MBq of [99m]TcO$_4^-$ dissolved in 2 ml 0.9% NaCl was added to the sealed kit vial and heated to 95 °C for 10 min. Subsequently, 10 µl of a 10 mM solution of the CIM compound was added to 500 µl of the ^{99m}Tc kit solution and heated to 95 °C for 20 min. The labeling reaction was followed by radio HPLC (0 – 100% MeCN in water within 5 min, Monolith column).

[99m]Tc-labeling of DTPA-conjugate

To label the DTPA-conjugate with ^{99m}Tc, 10 µl of a 1 mM DTPA-conjugate solution were mixed with 20 µl of 0.2 M phosphate buffer (pH = 9), 2 µl of DMSO and 10 µl of a solution containing 2 mg/ml SnCl$_2$. Finally, approximately 40 MBq of [99m]TcO$_4^-$ in 0.9% sodium chloride were added and everything was incubated at 95 °C for 20 min. The labeling was checked by radio HPLC (0 – 100% MeCN in water within 5 min, Monolith column).

[68]Ga-labeling of DOTA, NOTA, CHX-A''-DTPA, PCTA, oxo-DO3A and NODAGA-conjugates

For the PET scans, all capable compounds were labeled with [68]Ga. About 100 µl of ^{68}Ga chloride solution containing approximately 100 MBq were eluted from a [68]Ge/^{68}Ga generator with 0.6 M HCl. 34 µl NaOAc buffer and 1 µl of a 10 mM solution of the compound in DMSO was added, the pH was adjusted to 3.6 to 4 and the mixture was incubated for 5 min at 95 °C. If a high specific activity was required, 2 µl of a 1 mM solution of the compound were added. The labeling was checked using radio HPLC (0 - 100% MeCN in water within 4 min, Monolith column). In cases the labeling achieved purity below 95%, the product was purified using a SOLA cartridge. Washing was performed with a 0.9% NaCl solution and for elution ethanol was used. The ethanol then was vaporized and the remaining product was dissolved in 100 µl of a 0.9% NaCl solution and 10 µl of phosphate buffer.

NAALADase Assay

Recombinant human PSMA (rhPSMA, R&D systems, Wiesbaden, Germany) was diluted to 0.4 µg/ml in assay buffer (50 mM HEPES, 0.1 M NaCl, pH 7.5). The substrate Ac-Asp-Glu was diluted to yield a concentration of 40 µM in assay buffer. The tested, non-labeled compounds were prepared to obtain a volume of 30 µl with concentrations of 0 to 1000 nM in assay buffer. Firstly, 60 µl of rhPSMA solution and secondly, 30 µl of substrate solution were added to each prepared concentration of the tested compounds. The mixture was incubated at 37 °C for one hour and then the reaction was stopped by heating to 95 °C for 15 minutes. 120 µl of a 15 mM solution of *ortho*-phthaldialdehyde (OPA) in OPA Buffer (0.2 M NaOH, 0.1% β-mercaptoethanol (v/v)) were added to each vial and incubated for 10 minutes at room temperature. 100 µl aliquots of the reaction solution were given onto a F16 Black Maxisorp Plate (Nunc, Langenselbold, Germany) and read at an excitation wavelength of 330 nm and an emission wavelength of 450 nm using a microplate reader (DTX-880, Beckman Coulter, Krefeld, Germany). Data analysis was performed using the one-site total binding regression algorithm of GraphPad Prism. Each compound was measured at least three times.

Determination of the IC$_{50}$ values on LNCaP cells

A filter plate MultiScreen$_{HTS}$-DV was incubated at room temperature with 100 µl PBS with 1% BSA per

well for 30 min. After removing the PBS/BSA solution, 10^5 human prostate adenocarcinoma cells (LNCaP cells) in 50 µl of Opti-MEM (Life Technologies GmbH, Darmstadt, Germany) were applied to each well. Different concentrations of the non-labeled compounds (leading to concentrations of 0, 0.5, 1, 2.5, 5, 10, 25, 50, 100, 500, 1000 and 5000 nM in each well) in 300 µl of Opti-MEM were mixed with 3 µl of a 150 nM solution of ^{125}I-labeled MIP – 1095 in Opti-MEM. 50 µl of the resulting solution were added to each well, each concentration was pipetted in quadruples. Each well now contained the radiolabeled ligand in a concentration of 0.75 nM and the competitive, non-labeled ligand in the concentration mentioned above. The plate was then incubated for 45 min at room temperature on a shaker.

After the incubation, the cells were washed 2 × with 100 µl of ice cold PBS and 1 × with 200 µl of ice cold PBS. Finally, the filters were collected and the remaining radioactivity was measured with a gamma counter. Each tube was measured for 5 min.

Determination of the ratio of internalization

Two 24-well plates were coated with poly-L-lysine by incubating them with PBS containing 0.1% poly-L-lysine for 20 min at room temperature. The solution was then taken off and each well was washed with 1 ml of PBS. Next, 1 ml of a cell suspension was added to each well. It contained 10^5 LNCaP cells suspended in RPMI medium that included 10% fetal calf serum and 1% L-glutamine. The plates were incubated at 37 °C overnight.

The respective ^{177}Lu-labeled compound was incubated with the cells under four different conditions: at 37 °C with and without blocking of the receptor and at 4 °C with and without blocking of the receptor. Each sample was measured in triplets. The blocking was achieved by adding 2-(phosphonomethyl)pentanedioic acid (2-PMPA, Tocris Bioscience, Bristol, UK) in a concentration of 500 µM.

In detail, 99% Opti-MEM was mixed with 0.05% of a 6 µM solution of the radiolabeled ligand and with 0.05% of either 2-PMPA for the blocked fractions or DMSO for the others. 250 µl of this solution that contained the radiolabeled compound in a concentration of 30 nM was added to each well after the medium was removed. The plates were then incubated for 45 min at 37 °C in a water bath or at 4 °C on ice to inhibit the internalization.

Next, the supernatant was taken off and the cells were washed 4 × with ice cold PBS. 500 µl of a 50 mM glycine buffer at a pH of 2.8 was added to each well and incubated for 5 min at room temperature and ice

respectively. The supernatant was collected as the first washing sample. Again, 500 µl of the glycine buffer were added to each well, incubated for 5 min and collected as the second washing sample. The cells were washed once with ice cold PBS and finally lysed by adding 500 µl of a 0.3 M solution of sodium hydroxide and incubating it for 10 min at room temperature and ice, respectively. The solution was then collected as the lysis sample. Finally, a standard was created by taking 25 µl of the 30 nM solution of the radioactive ligand. All samples were measured in a gamma counter for 1 min each.

Organ distribution

Organ distribution was carried out in BALB/c nude mice LNCaP xenografts anesthetized with 2% sevoflurane. 10 nmol of the DOTA and CHX-A''-DTPA conjugates labeled with approximately 80 MBq of ^{68}Ga at a specific activity of 10 MBq/nmol were injected intravenously into the tail vein of five mice each. The mice were sacrificed after 1 h. All organs were dissected, weighed and the remaining radioactivity was measured in a gamma counter for 1 min each.

MicroPET

All compounds capable of chelating ^{68}Ga (this includes the DOTA, NOTA, CHX-A''-DTPA, PCTA, oxo-DO3A and NODAGA conjugates) were shown to be readily radiolabelled. The solutions containing the purified ^{68}Ga-labeled conjugates of DOTA and CHX-A''-DTPA (specific activity: 50 MBq/nmol) were sterile-filtered before 100 µl of the respective solution was injected into a BALB/c nude mouse LNCaP xenograft anesthetized with 2% sevoflurane, intravenously into the tail vein. After recording a one hour uptake kinetic microPET scans were gathered for up to 180 minutes with a Siemens Inveon PET scanner. In order to obtain a reliable comparison of both tracers the time dependency of the mean SUVs was plotted based on the reconstructed data.

PET/CT

The first-in-man PET/CT examination was carried out on a Biograph 6 PET/CT scanner (Siemens/CTI). Acquisition of the images was started 60 ± 10 min and 180 ± 10 min after intravenous injection of the ^{68}Ga-labeled conjugates containing HBED-CC and CHX-A''-DTPA, respectively. A specific activity of 50 MBq/nmol was used. The applied doses were 330 MBq ^{68}Ga tagged to 2 nmol HBED-CC ligand and 360 MBq ^{68}Ga tagged to 3 nmol CHX-A''-DTPA ligand. For attenuation correction of the PET scan, a CT scan (130 keV, 30 mAs; CareDose) without contrast medium was performed.

Results

Chemistry

The synthesis of the basic scaffold and coupling of the chelators was achieved by solid phase synthesis as described before [27]. Coupling of the chelators had to be adapted for each reaction to yield high amounts up to 95 % overall yield of the product. The detailed reaction conditions for each chelator are listed in table 1. After purification, all compounds achieved purities higher than 95% as determined by HPLC. Table S1 summarizes all necessary analytical data and HPLC results of all conjugates are shown in figure S1.
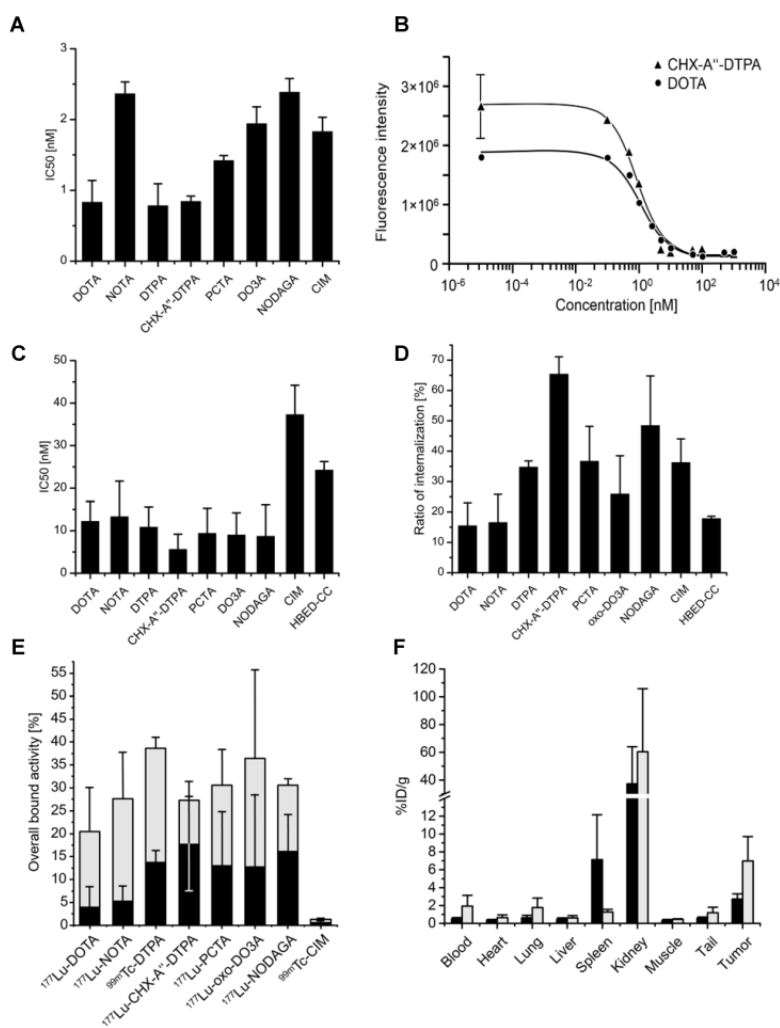

Figure 2: A In vitro IC_{50} values of <chelator>-conjugates determined by binding to purified rhPSMA (NAALADase assay). Labeling refers to the chelating entity coupled to the Glu-urea-based scaffold. **B** Exemplary fitting of the raw data of NAALADase assay, shown are the compounds coupled to DOTA (PSMA-617 currently in first-in-man studies) and CHX-A''-DTPA. **C** IC_{50} values determined by competitive binding on LNCaP cells. **D** Ratios of internalization. All compounds were labeled with ^{177}Lu except for DTPA and CIM which were labeled with ^{99m}Tc and HBED-CC conjugate (PSMA-11) which was labeled with ^{68}Ga. MIP-1095 is radiolabeled with ^{125}I. The CHX-A''-DTPA conjugate proved significance (one way ANOVA, $p < 0.05$) in comparison to all compounds except for the NODAGA conjugate. **E** Overall bound activity. The graph indicates the absolute amount of compound internalized (black) and surface-bound (grey), respectively, during internalization assay. **F** Organ distribution of the ^{68}Ga-CHX-A''-DTPA conjugate (black) and the ^{68}Ga-DOTA-conjugate (grey) in LNCaP tumor-bearing mice.

Radiolabeling

Radiochemical yields were determined to be >95% by radio-HPLC. All compounds incorporated the radiometals readily. ^{177}Lu labeling was achieved with a precursor amount of 10 nmol, incubated for 10 min at 95 °C leading to a specific activity of approximately 10 MBq/nmol. Labeling with ^{68}Ga was performed with either 10 nmol leading to a specific activity of 10 MBq/nmol or with 2 nmol, yielding a specific activity of 50 MBq/nmol of the precursor. The reaction mixture was incubated for 5 min at 95 °C.

NAALADase Assay

The binding affinities of the compounds to rhPSMA were expressed as their 50% inhibitory concentrations (i.e. IC_{50} values). The IC_{50} values ranged from 0.8 to 2.4 nM as shown in figure 2A. The best values were obtained for the DTPA, CHX-A''-DTPA and DOTA conjugate (0.8 ± 0.3 nM, 0.8 ± 0.1 nM and 0.8 ± 0.3, respectively).

Competitive Cell Binding

IC_{50} values on cells ranged from 5.6 nM for the compounds coupled to CHX-A''-DTPA to 37.3 for the CIM coupled construct (see figure 2C). The DOTA-conjugate PSMA-617 (IC_{50} = 12.2 ± 4.6 nM) and the HBED-CC-conjugate PSMA-11 (24.3 ± 2.0) are currently used in first-in-man studies and values obtained in this study match the published data [27, 33]. The CIM- and the HBED-CC-conjugate showed two-digit nanomolar affinities as compared to the one-digit nanomolar and subnanomolar affinities determined for the compounds analyzed in this study.

Internalization ratios

The ratios of internalization are shown in figure 2D. The values were obtained by setting the total amount of compound bound to the cells as 100% and then calculating the portion internalized into the cells. The DOTA conjugate and the HBED-CC conjugate intensely studied in current and former studies show the lowest values (15.5 ± 7.5% and 17.9 ± 0.7%, respectively). The highest ratios of internalization were found for the CHX-A''-DTPA conjugate (65.4 ± 5.7%) and the NODAGA conjugate (48.5 ± 16.4%). Absolute values for the amount of

compound bound to the cells can be seen in figure 2E. Overall, the amount of bound tracer is comparable, only the CIM conjugate shows scarcely any binding. Although there are conjugates that show higher overall binding, the CHX-A''-DTPA conjugate also obtained the highest absolute value of compound inside of the cells with 17.4 ± 10.8%. The CIM conjugate (0.46 ± 0.12%) and the DOTA conjugate (3.7 ± 4.6%) showed the lowest amounts of internalized compound.

Organ distribution

Values obtained for each organ underwent a half-life correction. The DOTA-coupled conjugate PSMA-617 and the CHX-A''-DTPA conjugate showed enrichment in tumor and kidneys as shown in figure 2F. Although the amount of tracer in the tumor is higher for the DOTA conjugate, the tumor to blood ratios are in the same order of magnitude (7.9 for the ^{68}Ga-labeled DOTA conjugate PSMA-617 vs 6.0 for the ^{68}Ga-labeled CHX-A''-DTPA conjugate).
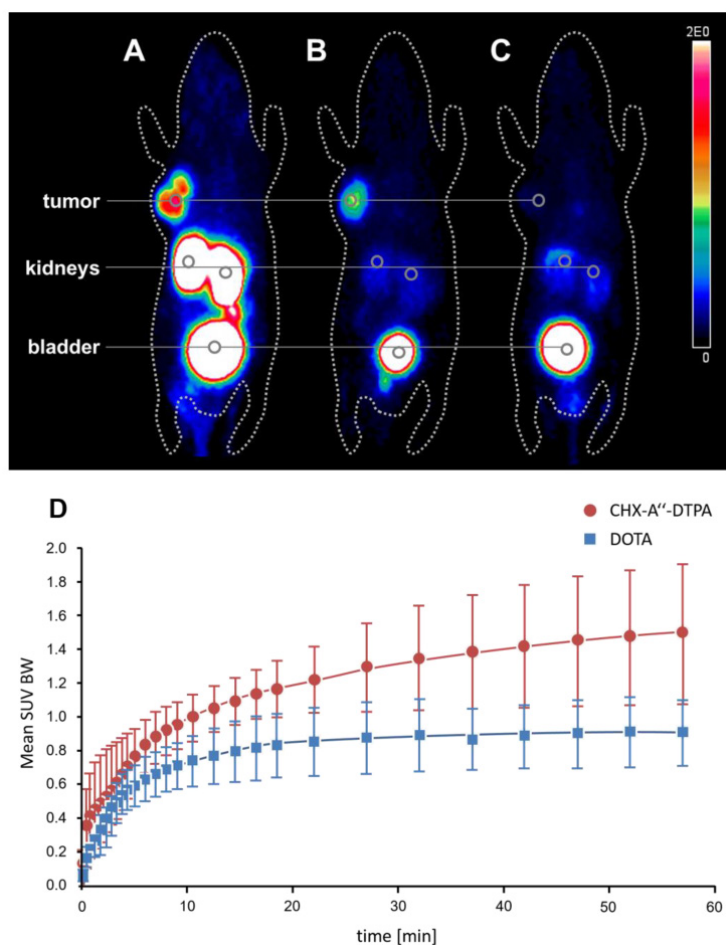

Figure 3: MicroPET comparison of the ^{68}Ga-labeled CHX-A''-DTPA conjugate **A** and the ^{68}Ga-labeled DOTA conjugate **B** in the same mouse. Both MIPs were recorded 2 h post injection. **C** MicroPET image (MIP) of the ^{68}Ga-labeled CHX-A''-DTPA conjugate blocked with 100-fold excess of the non-labeled compound 2 h post injection. **D** Tumor uptake dynamics of the first 60 minutes post injection of the ^{68}Ga-labeled conjugates coupled to DOTA and CHX-A''-DTPA.

MicroPET

To take the examination one step further the tumor uptake and pharmacokinetics of the ^{68}Ga labeled CHX-A''-DTPA conjugate was studied in an LNCaP-Xenograft. The results were compared to the ^{68}Ga-labeled DOTA conjugate. The PET scans taken 2 h post injection are shown in figure 3A and 3B, respectively. The scan shows enrichment of the compounds in the kidneys and in the bladder, a behavior that is known for all urea-based PSMA inhibitors. The kidney uptake is higher for the CHX-A''-DTPA conjugate. High tumor uptake can be seen, nonetheless, the uptake of CHX-A''-DTPA is remarkably higher. The dynamic behavior of both compounds during the first 60 minutes after injection is shown in figure 3D. While the amount of ^{68}Ga-labeled DOTA conjugate in the tumor begins to decrease after approximately 15 min, the amount of ^{68}Ga-labeled CHX-A''-DTPA conjugate increases until 60 min after injection and even further until the end of investigation (3 h post injection) as shown in table S2.

Blocking of the receptor by addition of 100-fold excess of the non-labeled compound prevents the tumor uptake of the ^{68}Ga-labeled CHX-A''-DTPA conjugate as shown in figure 3C.

PET/CT

Following the promising results from in vitro and in vivo testing for the CHX-A''-DTPA conjugate, we were able to obtain a first-in-man image using the ^{68}Ga-labeled compound in PET/CT. The image was compared to a PET/CT of the ^{68}Ga-labeled HBED-CC conjugate in the same patient as shown in figure 4. The PET/CT scans were obtained exactly one week apart. As most PCa tumors show a relatively low proliferation rate, tumor spread should be comparable during this interval.

The 68-year-old patient had undergone previous prostate surgery due to carcinoma and had received anti-androgen therapy with goserelin and bicalutamide since 2008. He also had history of percutaneous radiation therapy of several bone lesions, medication with zoledronic acid and chemotherapy with docetaxel. After developing lung metastases, he received 4 cycles of ^{177}Lu-PSMA617 and initially responded well. When the patient became progressive under that therapy, he was evaluated for a CHX-A''-DTPA PSMA-ligand with clinical indication. As this chelator is well suited for labeling with ^{213}Bi [34], an alpha emitter already proven to break

radioresistency against beta-emitters in patients [35], this combination might open new therapeutic options for this particular patient.
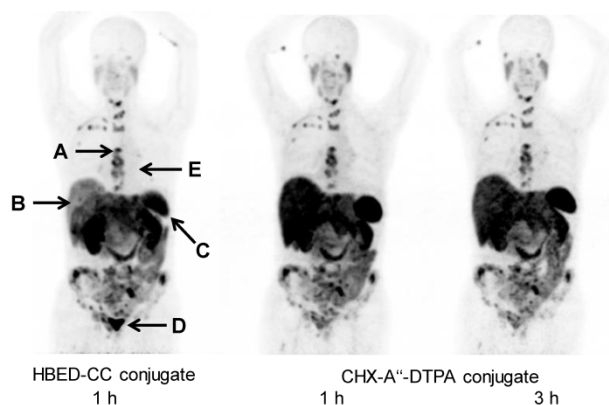

Figure 4: PET/CT scans (MIP) with the 68Ga-labeled PSMA binding conjugates containing the chelator HBED-CC and CHX-A''-DTPA. The arrows indicate reference lesions for further evaluation (see table 2)

Table 2: Maximum SUV determined using organ-volume of interest (VOI) analysis

	SUV max (organ-VOI)	HBED-CC 1 h	CHX-DTPA 1 h	CHX-DTPA 3 h
A	Bone metastases (sternum)	6.6	6.1	7
B	Liver	3.1	6.1	6
C	Spleen	8.2	16.3	16.2
D	Blader/urin	74	4.7	3.7
E	Blood-pool	1.1	1.9	1.8

Discussion

Until now, somatostatin receptor (SSTR) mediated endoradiotherapy remains the prototype of theranostic treatments. [36, 37] Based on the current progress in the field of PSMA related diagnostic imaging, and due to the high number of patients suffering from hormone refractory metastasized PSMA related therapies might even outperform the clinical value of SSTR binding tracers. This is of particular interest as PSMA ligands target prostate carcinoma, a tumor entity of high clinical relevance. The previous clinical results show excellent tumor targeting and therefore present a robust basis to achieve therapeutic efficacies. [11, 24, 25, 31, 38] As tumor cell internalization is a key factor for the efficiency of therapeutic radiopharmaceuticals, the currently available tracers still have to be optimized. Two components are known to define the performance of PSMA targeting tracers, namely the Glu-urea-based binding motif causing receptor binding and the spacer mediating a secondary interaction with the lipophilic surface next to the zinc containing binding pocket which simultaneously influences the pharmacokinetics. Here, we succeeded in determining the influence of the chelating entity on the tumor cell internalization of the compound. Besides high binding affinity, this is crucial for the therapeutic component of the theranostic concept of PSMA targeting to treat metastasized, hormone-refractory prostate carcinoma.

As a highly specific PSMA-binding motif was already found in earlier studies [20] and a current study presented a linker that showed the best performance *in vitro* and *in vivo* [33], the focus of this investigation was to determine the most suitable chelator. The different chelator-conjugates were screened with respect to their compound-receptor interaction on the recombinant receptor and cell based binding followed by internalization studies. These two different approaches to determine IC_{50} values were utilized to study the interaction of the compounds on two different levels. First, the NAALADase assay which examines the sheer receptor-compound interaction was conducted. The IC_{50} values obtained by this assay yield more precise values considering that there are no disruptive factors involved. Consequently, these IC_{50} values are generally lower than those measured on LNCaP cells. The competitive binding assay on LNCaP cells represents binding in the cellular context. The values received presumably provide more realistic conditions as they involve varying factors such as the receptor density and interaction with other proteins present. While the improvement of the internalization was shown significant for the CHX-A''-DTPA conjugate over all compounds except for the NODAGA conjugate, it should be mentioned that this improvement could be shown for several of the compounds studied. This highlights the influence of the chelating agent on the internalization. *In vivo* testing was carried out by means of microPET imaging. The ideal compound will combine a binding affinity and tumor targeting comparable to the DOTA conjugate PSMA-617 with a considerable higher ratio of internalization.

Of all the compounds tested, the CHX-A''-DTPA conjugate showed the most pronounced performance in this respect. Figure 5A shows a comprehensive overview of the internalization and the competitive binding assay *in vitro*. Most importantly, the internalization potency determined for the CHX-A''-DTPA conjugate was remarkably higher than that of all other compounds as seen in both, the relative and the absolute values. As the ratios of internalization differed more significantly than the IC_{50} values, we theorized that the chelator would especially influence the ratio of internalization if it provides hydrophobic residues (see figure 5C).

Therefore, we plotted the hydrophobicity of the tested compounds, depicted by the retention time in HPLC, against the performance in the internalization assay. Increasing hydrophobicity correlates with higher internalization (figure 5B). On the other hand this plot revealed that there is more to the internalization avidity than only the lipophilicity: The compound coupled to CHX-A''-DTPA showed a higher internalization ratio as expected when approximated by its hydrophobicity. This indicates specific interactions of the residues in CHX-A''-DTPA to the receptor in the process of internalization. This was further proven by implementation of the CIM conjugate, a highly lipophilic compound into the group of derivatives. This highly hydrophobic compound performed worst in nearly all assays conducted.

Encouraged by these findings, we decided to examine the biodistribution behavior of the tested compounds. PET scans of mouse xenografts that were injected with the ^{68}Ga-labeled CHX-A''-DTPA conjugate showed PSMA-specific enrichment of the radioactivity in the tumor. As expected the compound also accumulates in the kidneys (see figure 3A and B). This is known for PSMA inhibitors as PSMA is also found on the proximal tubular cells of the kidneys [10].

To examine the pharmacokinetics of CHX-A''-DTPA, the most promising compound, the biodistribution of the DOTA and the CHX-A''-DTPA conjugate was studied in LNCaP tumor bearing mice. Both compounds showed high enrichment of the tracers in the kidneys and the tumor. The values obtained for DOTA were higher in both of these tissues. Nevertheless, tumor-to-blood ratios obtained were comparable (tumor-to-blood = 5.43 in case of the CHX-A''-DTPA derivative and 3.62 in case of the DOTA derivative). As LNCaP tumors unfortunately often show highly varying properties, an intra-animal comparison using microPET of DOTA and CHX-A''-DTPA was performed as shown in figure 3A and B. Again, both compounds showed high tumor uptake. Interestingly, the tumor values for the CHX-A''-DTPA conjugate increased until the end of the investigation period (3 h post injection), while the tumor values of the DOTA conjugate peaked after the initial distribution phase and subsequently fell off. Kidney values decreased rapidly for the DOTA conjugate, but slowly for the CHX-A''-DPTA conjugate. In summary, these results show a benefit for the CHX conjugate with respect to tumor uptake and most importantly tumor retention while the DOTA conjugate provides an improved behavior with respect to its renal clearance.
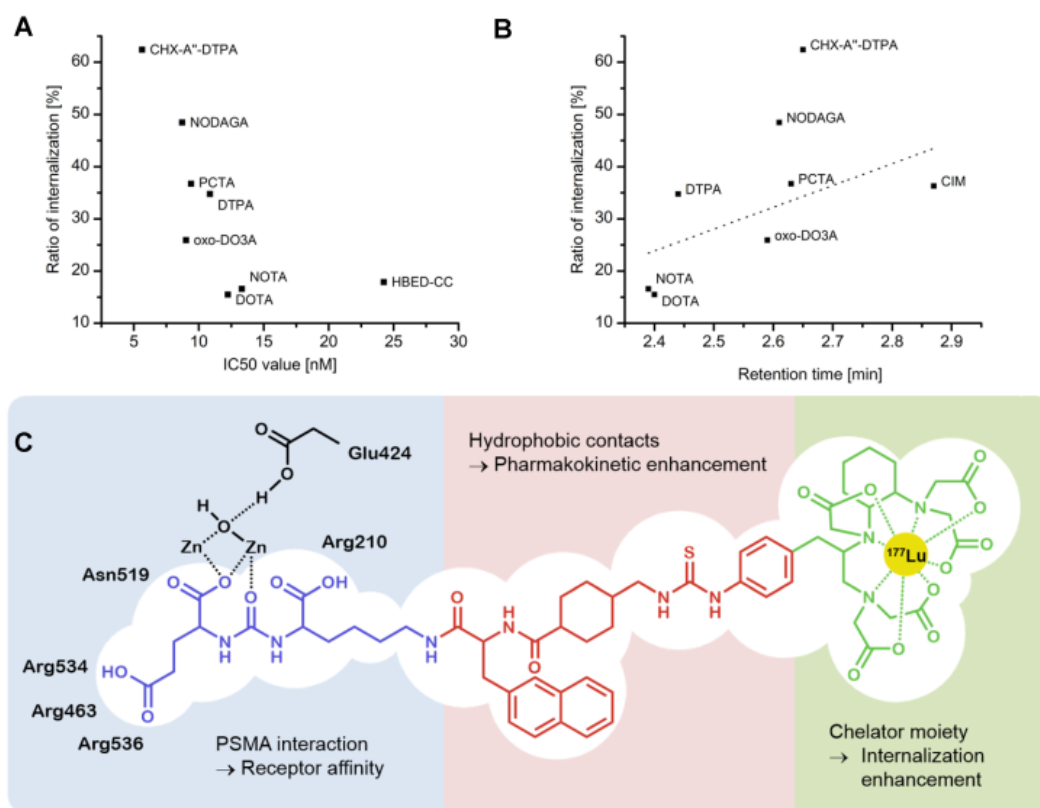

Figure 5: A Comparison of ratio of internalization and IC_{50} values of each compound. The compound coupled to CHX-A''-DTPA performed best in both assays and may therefore be a promising new compound. **B** Comparison of internalization ratio and retention time. The linear fit represents the correlation of internalization with increasing hydrophobicity (Pearson R value = 0.60). **C** Suggested model of action of the CHX-A''-DTPA-coupled ligand at the PSMA receptor. While the urea-based binding motif and the linker region seem to play primarily a crucial role in targeting the tumor, the chelating entity may have an essential part by enhancing internalization of the compound.

The excellent tumor retention of CHX-A''-DTPA combined with the fact that it may be capable of breaking radioresistance due to being capable of chelating the alpha-emitter ^{213}Bi justified a first-in-man application using the ^{68}Ga-labeled CHX-A''-DTPA compound for PET/CT. The obtained PET/CT scans indicated that the PSMA-specific compound enriches in the tumor and in the metastases. Variation of tumor uptake mediated by the PSMA binding motif was within ± 10% between both tracers, there was no difference in the number of lesions detected. Remarkably, the SUVmax value in the tumor showed a slight increase from one to three hours post injection for the CHX-A''-DTPA conjugate, replicating the tumor uptake behavior seen in the LNCaP tumor bearing mice in microPET. Additional accumulation can be observed in liver, spleen and in the salivary glands. Uptake in liver and spleen was approximately 2-fold higher for the CHX-A''-DTPA conjugate in comparison to the HBED-CC conjugate, the tracer in use for diagnostic examinations of patients suffering from PCa. Simultaneously, urine-clearance of the CHX-A''-DTPA conjugate was dramatically reduced and blood/soft-tissue residency time prolonged. This implicates a combined renal and hepato-faecal clearance of the CHX-A''-DTPA conjugate in comparison to the predominantly renal clearance for the non-tumor-bound HBED-CC conjugate. In particular, enrichment in kidneys is still the main dose-limiting factor of radiolabeled PSMA inhibitors used for endoradiotherapy. This combined with the fact that the CHX-A''-DTPA conjugate shows extraordinary tumor uptake but also high off-target accumulation, a displacement strategy as studied recently with 2-(phosphonomethyl)pentanedioic acid (PMPA) [39] to protect the kidneys might further enhance the potential of this candidate. The PET/CT imaging revealed comparatively high uptake in the spleen and the liver. Fortunately, these organs are not very sensitive to radiation [40]. This has been experienced in therapies of neuroendocrine tumors: ^{68}Ga-DOTATATE is known to suffer from high spleen and liver uptake [41]. However, in contrast to its high kidney uptake, representing the dose limiting factor of endoradiotherapy with DOTATATE, neither the liver nor the spleen uptake cause known side effects.

In conclusion the data presented reveal the importance of internalization potency for the development of PSMA binding tracers. It could be shown that - as exemplified for the CHX-A''-DTPA conjugate - the chelator moiety can be used to trigger a progressive long term accumulation in LNCaP mice, a behavior not observed to date. This might be of high relevance as the chelator CHX-A''-DTPA is capable of stably chelating several radiometals that can be used

for therapeutic and diagnostic purposes, for example ^{68}Ga, ^{177}Lu, ^{90}Y, ^{111}In and ^{213}Bi [34, 42-44]. These properties indicate that compounds comprising the Glu-urea-based binding motif in combination with hydrophobic linkers such as the chelator CHX-A''-DTPA represent promising candidates for prostate cancer therapy.

Supplementary Material

Supplementary tables and figures.
http://www.thno.org/v06p1085s1.pdf

Author contributions

Till Wüstemann contributed in conducting most of the experiments, writing of the manuscript and data interpretation. Ulrike Bauder-Wüst contributed in collaborating in carrying out the *in vitro* experiments and in the data interpretation and analysis of these. Martin Schäfer contributed to the syntheses of the compounds. Matthias Eder was involved in the design of the study and evaluation of the experiments. Martina Benesova was involved in the design of the study and evaluation of the experiments. Klaus Kopka gave scientific advice for the design of *in vivo* experiments. Karin Leotta contributed in conducting the microPET experiments. Clemens Kratochwil conducted the PET/CT scans of the first-in-man experiments. Uwe Haberkorn gave scientific advice for the design of the first-in-man experiments. Walter Mier planned the project, contributed to the design of the experiments and directed the preparation of the manuscript. All authors approved the manuscript.

Competing Interests

The authors have declared that no competing interest exists.

References

1. Schröder FH, Hugosson J, Roobol MJ, Tammela TLJ, Ciatto S, Nelen V, et al. Prostate-Cancer Mortality at 11 Years of Follow-up. New England Journal of Medicine. 2012; 366: 981-90.
2. Giovacchini G, Picchio M, Garcia-Parra R, Briganti A, Abdollah F, Gianolli L, et al. 11C-Choline PET/CT Predicts Prostate Cancer–Specific Survival in Patients with Biochemical Failure During Androgen-Deprivation Therapy. Journal of Nuclear Medicine. 2014; 55: 233-41.
3. Tilki D, Reich O, Graser A, Hacker M, Silchinger J, Becker AJ, et al. 18F-Fluoroethylcholine PET/CT Identifies Lymph Node Metastasis in Patients with Prostate-Specific Antigen Failure After Radical Prostatectomy but Underestimates Its Extent. European Urology. 2013; 63: 792-6.
4. Vorster M, Modiselle M, Ebenhan T, Wagener C, Sello T, Zeevaart JR, et al. Fluorine-18-Fluoroethylcholine PET/CT in the detection of prostate cancer: A South African experience. Hell J Nucl Med. 2015; 18: 53-9.
5. Kirby M, Hirst C, Crawford ED. Characterising the castration-resistant prostate cancer population: a systematic review. International Journal of Clinical Practice. 2011; 65: 1180-92.
6. Katzenwadel A, Wolf P. Androgen deprivation of prostate cancer: Leading to a therapeutic dead end. Cancer Letters. 2015; 367: 12-7.
7. Nozawa M, Mukai H, Takahashi S, Uemura H, Kosaka T, Onozawa Y, et al. Japanese phase I study of cabazitaxel in metastatic castration-resistant prostate cancer. Int J Clin Oncol. 2015: 1-9.

8. Silver DA, Pellicer I, Fair WR, Heston WD, Cordon-Cardo C. Prostate-specific membrane antigen expression in normal and malignant human tissues. Clinical Cancer Research. 1997; 3: 81-5.
9. Ghosh A, Heston WDW. Tumor target prostate specific membrane antigen (PSMA) and its regulation in prostate cancer. Journal of Cellular Biochemistry. 2004; 91: 528-39.
10. Mhawech-Fauceglia P, Zhang S, Terracciano L, Sauter G, Chadhuri A, Herrmann FR, et al. Prostate-specific membrane antigen (PSMA) protein expression in normal and neoplastic tissues and its sensitivity and specificity in prostate adenocarcinoma: an immunohistochemical study using mutiple tumour tissue microarray technique. Histopathology. 2007; 50: 472-83.
11. Barrett JA, Coleman RE, Goldsmith SJ, Vallabhajosula S, Petry NA, Cho S, et al. First-in-Man Evaluation of 2 High-Affinity PSMA-Avid Small Molecules for Imaging Prostate Cancer. Journal of Nuclear Medicine. 2013; 54: 380-7.
12. Carter RE, Feldman AR, Coyle JT. Prostate-specific membrane antigen is a hydrolase with substrate and pharmacologic characteristics of a neuropeptidase. Proceedings of the National Academy of Sciences. 1996; 93: 749-53.
13. Bařinka C, Rojas C, Slusher B, Pomper M. Glutamate carboxypeptidase II in diagnosis and treatment of neurologic disorders and prostate cancer. Current medicinal chemistry. 2012; 19: 856.
14. Barrett AJ. Enzyme Nomenclature, Recommendations 1992. European Journal of Biochemistry. 1997; 250: 1-6.
15. Kawakami M, Nakayama J. Enhanced Expression of Prostate-specific Membrane Antigen Gene in Prostate Cancer as Revealed by in Situ Hybridization. Cancer Research. 1997; 57: 2321-4.
16. Liu H, Rajasekaran AK, Moy P, Xia Y, Kim S, Navarro V, et al. Constitutive and Antibody-induced Internalization of Prostate-specific Membrane Antigen. Cancer Research. 1998; 58: 4055-60.
17. Murphy GP, Maguire RT, Rogers B, Partin AW, Nelp WB, Troychak MJ, et al. Comparison of serum PSMA, PSA levels with results of cytogen-356 ProstaScint® scanning in prostatic cancer patients. The Prostate. 1997; 33: 281-5.
18. Heidenreich A, Bastian PJ, Bellmunt J, Bolla M, Joniau S, van der Kwast T, et al. EAU Guidelines on Prostate Cancer. Part 1: Screening, Diagnosis, and Local Treatment with Curative Intent—Update 2013. European Urology. 2014; 65: 124-37.
19. Troyer JK, Feng Q, Beckett ML, Wright Jr GL. Biochemical characterization and mapping of the 7E11-C5.3 epitope of the prostate-specific membrane antigen. Urologic Oncology: Seminars and Original Investigations. 1995; 1: 29-37.
20. Hillier SM, Maresca KP, Femia FJ, Marquis JC, Foss CA, Nguyen N, et al. Preclinical Evaluation of Novel Glutamate-Urea-Lysine Analogues That Target Prostate-Specific Membrane Antigen as Molecular Imaging Pharmaceuticals for Prostate Cancer. Cancer Research. 2009; 69: 6932-40.
21. Maresca KP, Hillier SM, Femia FJ, Keith D, Barone C, Joyal JL, et al. A Series of Halogenated Heterodimeric Inhibitors of Prostate Specific Membrane Antigen (PSMA) as Radiolabeled Probes for Targeting Prostate Cancer. Journal of Medicinal Chemistry. 2009; 52: 347-57.
22. Hillier SM, Kern AM, Maresca KP, Marquis JC, Eckelman WC, Joyal JL, et al. 123I-MIP-1072, a Small-Molecule Inhibitor of Prostate-Specific Membrane Antigen, Is Effective at Monitoring Tumor Response to Taxane Therapy. Journal of Nuclear Medicine. 2011; 52: 1087-93.
23. Afshar-Oromieh A, Zechmann CM, Malcher A, Eder M, Eisenhut M, Linhart HG, et al. Comparison of PET imaging with a 68Ga-labelled PSMA ligand and 18F-choline-based PET/CT for the diagnosis of recurrent prostate cancer. European Journal of Nuclear Medicine & Molecular Imaging. 2014; 41: 11-20.
24. Afshar-Oromieh A, Haberkorn U, Eder M, Eisenhut M, Zechmann CM. [Ga]Gallium-labelled PSMA ligand as superior PET tracer for the diagnosis of prostate cancer: comparison with F-FECH. European Journal of Nuclear Medicine & Molecular Imaging. 2012; 39: 1085-6.
25. Afshar-Oromieh A, Malcher A, Eder M, Eisenhut M, Linhart HG, Hadaschik BA, et al. PET imaging with a [68Ga]gallium-labelled PSMA ligand for the diagnosis of prostate cancer: biodistribution in humans and first evaluation of tumour lesions. Eur J Nucl Med Mol Imaging. 2013; 40: 486-95.
26. Eder M, Neels O, Müller M, Bauder-Wüst U, Remde Y, Schäfer M, et al. Novel Preclinical and Radiopharmaceutical Aspects of [68Ga]Ga-PSMA-HBED-CC: A New PET Tracer for Imaging of Prostate Cancer. Pharmaceuticals. 2014; 7: 779-96.
27. Eder M, Schäfer M, Bauder-Wüst U, Hull W-E, Wängler C, Mier W, et al. 68Ga-Complex Lipophilicity and the Targeting Property of a Urea-Based PSMA Inhibitor for PET Imaging. Bioconjugate Chemistry. 2012; 23: 688-97.
28. Hillier SM, Maresca KP, Lu G, Merkin RD, Marquis JC, Zimmerman CN, et al. 99mTc-Labeled Small-Molecule Inhibitors of Prostate-Specific Membrane Antigen for Molecular Imaging of Prostate Cancer. Journal of Nuclear Medicine. 2013; 54: 1369-76.
29. Afshar-Oromieh A, Avtzi E, Giesel FL, Holland-Letz T, Linhart HG, Eder M, et al. The diagnostic value of PET/CT imaging with the (68)Ga-labelled PSMA ligand HBED-CC in the diagnosis of recurrent prostate cancer. Eur J Nucl Med Mol Imaging. 2015; 42: 197-209.
30. Kratochwil C, Giesel F, Eder M, Afshar-Oromieh A, Benešová M, Mier W, et al. [177Lu]Lutetium-labelled PSMA ligand-induced remission in a patient with metastatic prostate cancer. Eur J Nucl Med Mol Imaging. 2015: 1-2.
31. Zechmann C, Afshar-Oromieh A, Armor T, Stubbs J, Mier W, Hadaschik B, et al. Radiation dosimetry and first therapy results with a 124I/131I-labeled small molecule (MIP-1095) targeting PSMA for prostate cancer therapy. Eur J Nucl Med Mol Imaging. 2014; 41: 1280-92.
32. Benesova M, Schaefer M, Bauder-Wuest U, Mier W, Haberkorn U, Eisenhut M, et al. Linker Modifications of DOTA-conjugated Inhibitors of the Prostate-Specific Membrane Antigen (PSMA). Eur J Nucl Med Mol Imaging: Springer 233 Spring St, New York, NY 10013 USA; 2013. p. S281-S.
33. Benešová M, Schäfer M, Bauder-Wüst U, Afshar-Oromieh A, Kratochwil C, Mier W, et al. Preclinical Evaluation of a Tailor-Made DOTA-Conjugated PSMA Inhibitor with Optimized Linker Moiety for Imaging and Endoradiotherapy of Prostate Cancer. Journal of Nuclear Medicine. 2015; 56: 914-20.
34. Nikula TK, McDevitt MR, Finn RD, Wu C, Kozak RW, Garmestani K, et al. Alpha-Emitting Bismuth Cyclohexylbenzyl DTPA Constructs of Recombinant Humanized Anti-CD33 Antibodies: Pharmacokinetics, Bioactivity, Toxicity and Chemistry. Journal of Nuclear Medicine. 1999; 40: 166-76.
35. Kratochwil C, Giesel FL, Bruchertseifer F, Mier W, Apostolidis C, Boll R, et al. 213Bi-DOTATOC receptor-targeted alpha-radionuclide therapy induces remission in neuroendocrine tumours refractory to beta radiation: a first-in-human experience. Eur J Nucl Med Mol Imaging. 2014; 41: 2106-19.
36. Kwekkeboom DJ, de Herder WW, Kam BL, van Eijck CH, van Essen M, Kooij PP, et al. Treatment With the Radiolabeled Somatostatin Analog [177Lu-DOTA0,Tyr3]Octreotate: Toxicity, Efficacy, and Survival. Journal of Clinical Oncology. 2008; 26: 2124-30.
37. de Jong M, Breeman WAP, Kwekkeboom DJ, Valkema R, Krenning EP. Tumor Imaging and Therapy Using Radiolabeled Somatostatin Analogues. Accounts of Chemical Research. 2009; 42: 873-80.
38. Weineisen M, Simecek J, Schottelius M, Schwaiger M, Wester H-J. Synthesis and preclinical evaluation of DOTAGA-conjugated PSMA ligands for functional imaging and endoradiotherapy of prostate cancer. EJNMMI Research. 2014; 4: 63.
39. Kratochwil C, Giesel FL, Leotta K, Eder M, Hoppe-Tich T, Youssoufian H, et al. PMPA for Nephroprotection in PSMA-Targeted Radionuclide Therapy of Prostate Cancer. Journal of Nuclear Medicine. 2015; 56: 293-8.
40. Rosler P, Christiansen H, Kortmann RD, Martini C, Matuschek C, Meyer F, et al. Hepatotoxicity after liver irradiation in children and adolescents : results from the RiSK. Strahlenther Onkol. 2015; 191: 413-20.
41. Walker RC, Smith GT, Liu E, Moore B, Clanton J, Stabin M. Measured Human Dosimetry of 68Ga-DOTATATE. Journal of Nuclear Medicine. 2013; 54: 855-60.
42. Baur B, Solbach C, Andreolli E, Winter G, Machulla H-J, Reske S. Synthesis, Radiolabelling and In Vitro Characterization of the Gallium-68-, Yttrium-90- and Lutetium-177-Labelled PSMA Ligand, CHX-A''-DTPA-DUPA-Pep. Pharmaceuticals. 2014; 7: 517-29.
43. Milenic DE, Garmestani K, Chappell LL, Dadachova E, Yordanov A, Ma D, et al. In vivo comparison of macrocyclic and acyclic ligands for radiolabeling of monoclonal antibodies with 177Lu for radioimmunotherapeutic applications. Nuclear Medicine and Biology. 2002; 29: 431-42.
44. Timmermand OV, Ulmert D, Evans-Axelsson S, Pettersson K, Bjartell A, Lilja H, et al. Preclinical imaging of kallikrein-related peptidase 2 (hK2) in prostate cancer with a (111)In-radiolabelled monoclonal antibody, 11B6. EJNMMI Research. 2014; 4: 51.